JOURNAL OF MATERIALS SCIENCE **37** (2002) 4545 – 4553

Identification of mass fractal in chemically synthesized ZnS quantum dots

W. VOGEL
Fritz-Haber-Institut der Max-Planck-Gesellschaft, Faradayweg 4-6, D-14195 Berlin, Germany

D. DHAYAGUDE
Department of Physics, University of Pune, Pune 411 007, India

R. CHITRA, D. SEN, S. MAZUMDER
Bhabha Atomic Research Centre, Trombay, Mumbai 400085. India

S. K. KULKARNI
Department of Physics, University of Pune, Pune 411 007, India
E-mail: skk@physics.unipune.ernet.in

Zinc sulphide quantum dots chemically capped with thioglycerol having two different sizes have been synthesized. The particles have a disordered sphalerite structure and are slightly contracted by 1% against the bulk. Small angle X-ray scattering investigations reveal that powders of these nanocrystallites are mass fractals that aggregate via a reaction-limited process to form irregular but rather dense networks with a fractal dimensionality of $D_f = 2.7$ and 2.1, respectively.

1. Introduction

Nanostructured materials form an important research area [1–5] and are being investigated extensively. As the materials approach a length scale of ∼100 nm, surface to bulk atoms ratio starts increasing which is quite useful in many catalytic reactions. Besides this straight forward effect of size reduction, Due to the presence of a small number of atoms, at this length scale, the properties of nanostructured materials cannot be described simply by those of single atoms, molecules or extended solids. Phenomenon of size dependent electronic structure of solids therefore leads to novel materials.

In case of semiconductors, as the dimensions of solids become comparable to the Bohr diameter of excitons, electron spectra change dramatically [1], affecting their optical and electronic properties. Due to the reduced dimensionality charge carriers are confined in space. Depending upon whether the confinement is in two dimensions (2D), one dimension (1D) or zero dimension (0D) semiconductor materials are referred to as quantum wells, quantum wires and quantum dots, respectively. The spectacular manifestation of charge confinement on electronic structure is the increase in band gap between valence and conduction band, discretization of energy levels and increase in the oscillator strength.

In order to investigate the semiconductor quantum dots or semiconductor nanoparticles usually two approaches are used. One approach is to start with the bulk solid and reduce it to the desired dimension employing lithographic technique. Another approach is to start with a small number of atoms or molecules as a nucleation centre and grow the solids employing variety of physical and chemical routes now developed. Nanoparticles synthesized using chemical methods have advantages that they can be investigated as colloidal particles in liquids and deposited as thin films from liquid having properties different from those of bulk materials. However, to obtain bulk solids or thin films from nanoparticles, retaining their nanoparticle properties, surface passivation of nanoparticles is mandatory. Surface passivation can be carried out using a variety of molecules [6] and procedures [7]. The procedure and molecules used in surface passivation as well as rates of removal of liquids may influence [8] the way in which nanoparticles form solids. Nanoparticles may grow by Ostwald ripening in which atoms, ions, or clusters keep on adding to a nucleation centre forming an extended solid. Alternatively nanoparticles may form self-assemblies of nanocrystallites producing a superlattice [9] or simply aggregate. Spanhel and Anderson [10] used fluorescence spectroscopy to investigate aggregation events in highly concentrated ZnO and CdS colloids. Korgel and Fitzmaurice [11], Kagan *et al*. [12] and Ptatshchek *et al*. [13] used Small Angle X-ray Scattering (SAXS) to investigate aggregation events in nanocrystals. It is interesting to investigate the growth of nanoparticles as it will have profound effects on the electronic structure and hence the properties.

We have synthesized zinc sulphide (ZnS) nanoparticles by a wet chemical approach in which the surfaces of the nanoparticles are passivated using thioglycerol (TG) molecules. Direct imaging methods like TEM, STM, or AFM are sometimes inadequate to investigate the way in which the powders are grown due to special sample preparation requirement of these techniques.

However, SAXS technique provides statistically averaged data, and is found to be adequate in order to follow the of growth or assembly of nanoparticles. SAXS has been successfully used earlier to investigate porous structures [14–17] as well as some nanoparticles [11–13]. By using SAXS we show that thioglycerol passivated ZnS nanoparticles have a fractal geometry.

2. Experimental

Synthesis of ZnS nanoparticles, having two different average sizes, were carried out using a chemical route. In this case aqueous solutions of zinc chloride ($ZnCl_2$) and unhydrous sodium sulphide (Na_2S) were reacted in the presence of thioglycerol or TG [$HSCH_2CH(OH)CH_2OH$]. Synthesis was carried out at room temperature. $ZnCl_2$ and TG were mixed in a reaction vessel and stirred continuously under nitrogen atmosphere. Na_2S was added drop-wise to the solution. After the reaction was completed the solution was stirred for sometime and then air-dried to get nanoparticles in the form of a white precipitate. The precipitate was thoroughly washed with water and air dried to obtain ZnS nanoparticles for the analysis. By varying the molarity of capping agent viz. TG, samples with different average sizes could be produced. Here two samples referred to as ZnS-1 and ZnS-3 are synthesized and used for the analysis.

For optical absorption measurements the samples were dispersed in double distilled water. Using double distilled water as a reference, spectra were recorded over a 200 nm to 500 nm range on a Hitachi UV-300 double beam spectrophotometer.

Small angle X-ray scattering (SAXS) measurements have been performed by a Kratky camera (Anton Paar) combined with a primary graphite monochromator and Cu $K_{\square 1}$ radiation. The scattered intensity was collected by a positional sensitive detector system (Braun). The powder samples were measured as received, and suspended on a thin 0.003 mm polyethylene foil. For each measurement a corresponding background scan of the empty foil was performed, and subtracted from the scan of the nano-ZnS. After background subtraction the patterns have been corrected for the slit height smearing [18].

The wide angle X-ray scattering (WAXS) experiments were performed with a Guinier counter diffractometer using a focussing Ge-111 Johanson-type monochromator and Cu $K_{\square 1}$ radiation (Huber). The diffractrograms have been corrected for the background scattering produced by the polyethylene foil and additional parasitic scattering. We have applied the usual angular factors (absoption, polarisation, geometric factors). All diffractograms are rescaled to the reciprocal scattering length $b (b = 2\sin(\theta)/\lambda$, 2θ: scattering angle $\lambda = 1.5404$ Å: wavelength).

Transmission Electron Microscopy (TEM) was performed with Philips 200 kV microscope equipped with a field emission gun, Philips CM 200 FEG. The coefficient of spherical aberration is $Cs = 1.35$ mm. The information limit for this instrument is better than 0.18 nm. The sample in the form of powders were dispersed in methanol. A drop of this solution was deposited on an amorphous carbon film of about 4 nm thickness and dried before it was inserted into the microscope. In addition to TEM images, electron diffraction images were also taken.

3. Results and discussion

Optical absorption spectra of ZnS-1 and ZnS-3 samples showed in Fig. 1 exhibit peaks at 260 nm and 290 nm respectively. Bulk ZnS solid has an energy gap [19] of 3.68 eV at 300 K. With an onset in optical absorption at ~345 nm. Observation of blue shift and rather sharp excitonic peaks in the optical absorption spectra for the present samples are characteristics of nanoparticles.

The wide angle X-ray diffraction of an assembly of particles is basically a superposition of the scattering of the individual particles independent of whether or not these particles form large aggregates. It therefore reveals the atomic structure (size, size distribution, crystal structure, disorder, etc.) of the basic nanoparticles of ZnS.

Fig. 2 shows the corrected wide angle X-ray scattering of sample ZnS-1. We used the so called Debye Function Analysis (DFA) to simulate the observed pattern. This method is described earlier in some details [20–23]. The model clusters used for this simulation are lattice fragments constructed by stacks of (111) planes, each containing $n \times m$ ZnS groups. The stacking of the (111) planes can be modified from ideal cubic, cubic with some stacking faults, to ideal hexagonal stacking [24]. As a result we obtain the symmetry and the size distribution of particles contributing to the diffraction effects. The particles have definitely the bulk cubic sphalerite symmetry (compare the sphalerite structure,

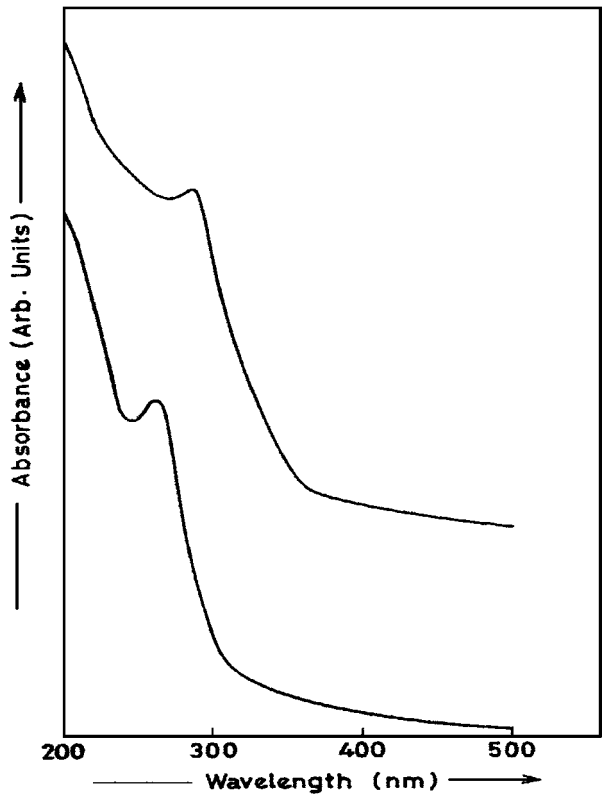

Figure 1 Optical absorption of ZnS-1 and ZnS-3 nanoparticle samples suspended in double distilled water.

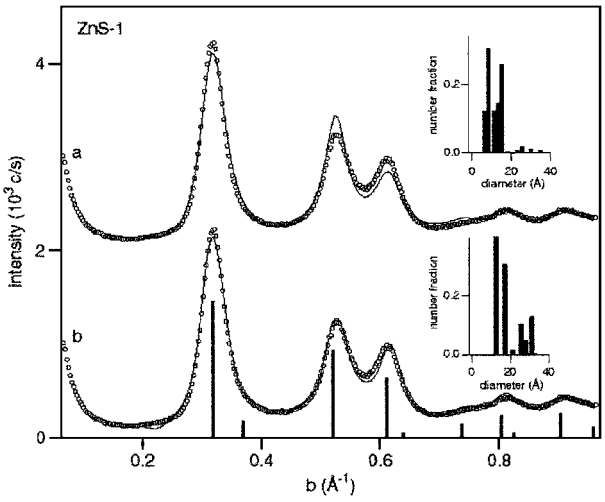

Figure 2 WAXS pattern of sample 1 (open symbols) compared with a simulation calculation by an assembly of twinned (bottom), and non-twinned (top) Sphalerite-type ZnS clusters (solid line). Vertical bars represent the structure factors of cubic ZnS. The size distributions of the model clusters are shown in the inserts.

vertical bars in Fig. 2). The simulation with a perfect cubic structure was less satisfying, especially for peaks 2 and 3 (curve a in Fig. 2, shown with offset). An improvement was achieved by the introduction of twin-defects. The (relative) R-factor

$$R = \left[\Sigma(I_{\text{exp}} - I_{\text{calc}})^2\right]^{1/2} / \Sigma I_{\text{exp}}$$

decreases from 0.86% to 0.55% in the latter case. In our simulation each model cluster contains one twin defect. The size distribution is narrow, with an average size around 20 Å, but smaller clusters with 12 Å size are also very frequent (40% by number). For the simulation with perfect cubic model clusters, however, the larger clusters between 20 to 30 Å are less frequent. This is related to a reduced coherence length along ⟨111⟩ if the scattering object contains a twin plane. The simulations performed with hexagonal wurtzite-type model clusters failed completely, and are not shown here. Simulations as shown in Fig. 2 are also performed for the sample ZnS-3. The results are similar, except that the latter has a larger average size.

A contraction/expansion $\delta a/a$ (a: bulk lattice constant) of the cluster matter is directly related to an expansion/compression of the scattering function in reciprocal space, i.e., $\delta a/a = -\delta b/b$. The value of δb can be determined with rather high precision in the DFA simulation [25]. Here we obtain a compression of $\delta a/a = -1 \pm 0.1\%$ for both samples against the bulk phase of ZnS, in agreement with earlier studies [24].

Since the ZnS clusters are not monodispersed the size averages weighted by number, by particle surface, and by the particle volume are different. The averages increase in this sequence with increasing degree of polydispersity. Table I contains the mean particle sizes from WAXS/DFA, weighted by their number, surface, and mass, respectively. According to this data sample ZnS-1 shows the lower polydispersity of the two samples.

Fig. 3 shows the SAXS pattern of samples ZnS-1 and ZnS-3 in a plot $b^2I(b)$ versus b. This type of

TABLE I Average sizes from WAXS for the two nano-crystalline ZnS samples. The averages increase depending on the weighting: the number average is smallest, the volume average largest. The differences indicate the degree of polydispersity

Sample	Average by number (Å)	Average by surface (Å)	Average by mass (Å)
ZnS-1	18.5	23.4	25.5
ZnS-3	29.0	40.1	44.1

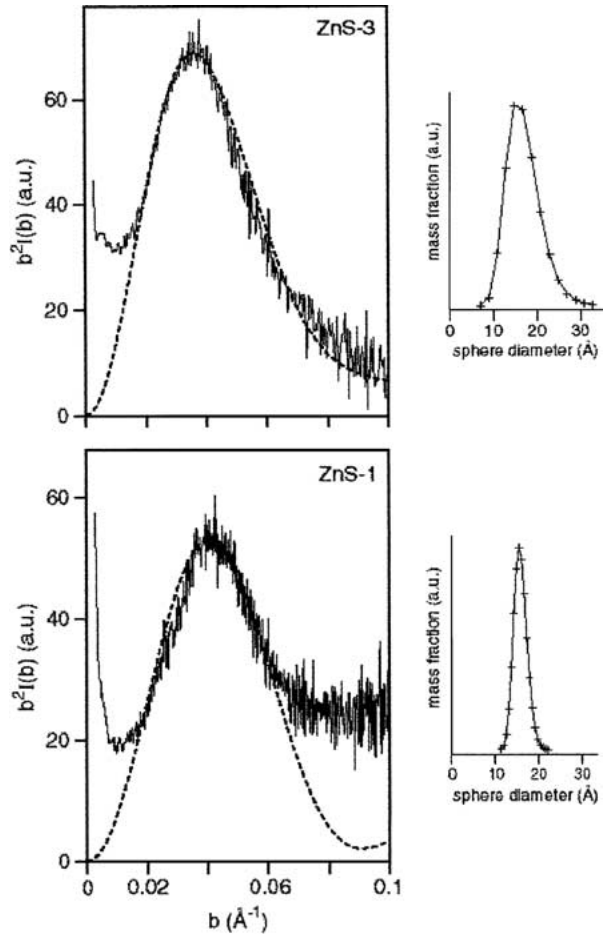

Figure 3 SAXS momentum plot of samples 1 and 3. The peaks are fitted using a log-normal distribution of spherical particles (dashed lines). The corresponding size distributions are shown on the right hand side.

'momentum-plot' is specially suited to analyze the continuous SAXS stemming from particle scattering [26]. In the Guinier approach [27] the particle scattering can be expressed as a Gaussian function: $I(b) \propto \exp(-ab^2)$. The momentum curve $b^2I(b)$ is zero at $b = 0$ and large b-values with an intermediate maximum at $b = a^{-2}$. Guinier's equation applies in the limit of $b \to 0$, independent of the particle shape, but restricts to a monodisperse system of particles. For a non-aggregated polydispersed particle system one expects a similar function, the maximum and width of which is defined by the size distribution function [26]. For simplicity, here we assume spherical shaped particles that are distributed at log-normal. The best fit of the calculated scattering intensity is shown in Fig. 3 as dashed lines. The log-normal distributions used for the fitting are displayed at the right side of Fig. 3.

A good fit is possible for the sample ZnS-3. The diffraction curves deviate, however, from the model of

independently scattering particles at the lowest angles. Also X-ray wide-angle scattering, which is not considered in this simulation, contributes to the intensity at the high angle end of the SAXS curve. This is more pronounced for sample ZnS-1. The mean particle sizes (sphere 'diameters') are 16 Å and 20 Å for ZnS-1 and ZnS-3, respectively. This is in fair agreement with the WAXS/DFA results. Within the limits of this analysis the width of the size distribution appears to be narrower for sample ZnS-1. As follows we will show that the proposition of independent scatterers is inadequate, and the deduced SAXS sizes must be taken with care.

The steep increase of the intensity at very low angles in Fig. 3 has its origin in the fractal nature of this material. The subject has been reviewed among others by P. W. Schmidt [28] and the scattering by fractals by Martin and Hurd [29] and references therein. Fig. 4 shows the observed intensity in a log-log scale, and in fact two regions with linear slopes can be distinguished (see dashed lines): at the high angle end the curves show the expected asymptotic 'Porod behavior' with a slope of $m = -4$. The Porod-law should be obeyed for a two-phase system with a 'sharp' density transition between the scattering objects and the surrounding medium [30, 31]. Bale and Schmidt [32] have shown that for fractal surfaces the Porod law is modified to $I(b) \sim b^{D_S-6}$. For a smooth surface D_s equals 2, but may be larger for a fractal 'rough' surface. This means that the ZnS particles seen by WAXS have a non-fractal surface morphology.

The linear range at the smallest angles have slopes of $m = -2.7$ (ZnS-1), and $m = -2.1$ (ZnS-3), respectively. In terms of the diffraction theory from fractal objects this observation is explained as scattering from mass fractals with fractal dimensions $D_f = 2.7$, and $D_f = 2.1$.

Schaefer *et al.* [33] studied colloidal silica aggregates using light and X-ray scattering. They obtained the same fractal dimension of 2.1 as observed for ZnS-3. In another SAXS study of silica aerogels with $D_f = 2.0$ the structure was described by a fractal backbone structure traced by the underlying chemical (polymerization) and physical (colloid aggregation) growth processes [34].

Two most popular models have been discussed: (i) diffusion-limited aggregation (DLA) [35, 36] yielding $D_f = 2.5$, independent of the sticking coefficients ($0.1 \leq s \leq 1$), and (ii) cluster-cluster aggregation

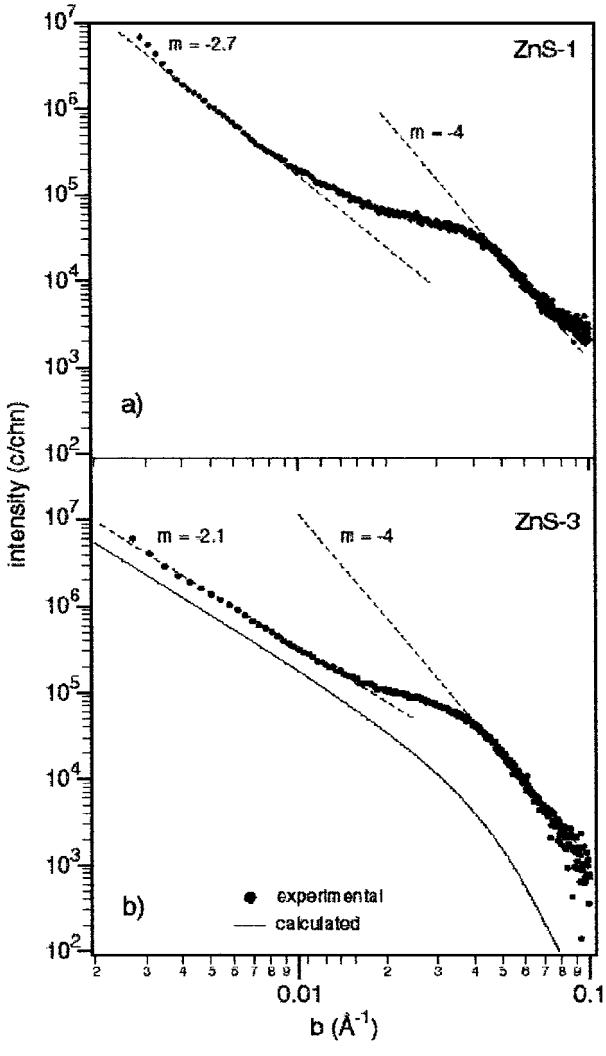

Figure 4 Log-log plot of the SAXS intensity of samples 1 and 3.

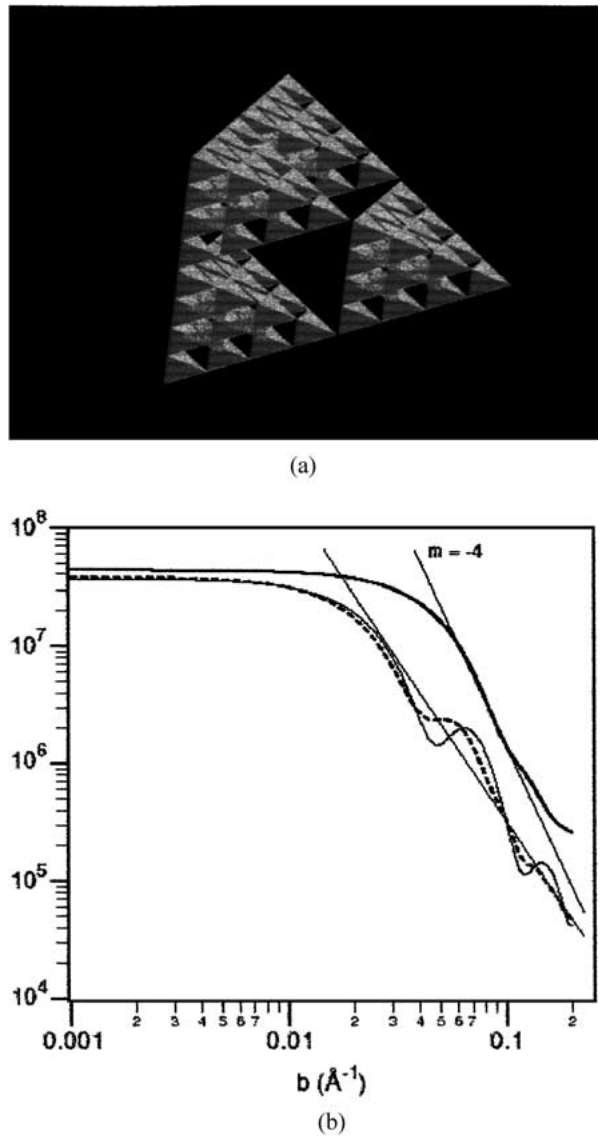

Figure 5 (a) Self-similar fractal object of 4 blocks of tetrahedral $Zn_{20}S_{35}$ with cubic Sphalerite symmetry. The outlined polyhedra are the ZnS_4 and SZn_4 Sphalerite units, respectively. The edge length of this fractal is 31 Å. (b) Log-log plot of the calculated SAXS intensity of the fractal tetrahedron in Fig. 5 (thin line), compared with the SAXS of an isolated $Zn_{20}S_{35}$ sub-unit (thick line). The dashed curve is for 4 randomly oriented $Zn_{20}S_{35}$ sub-units, linked over their vertices.

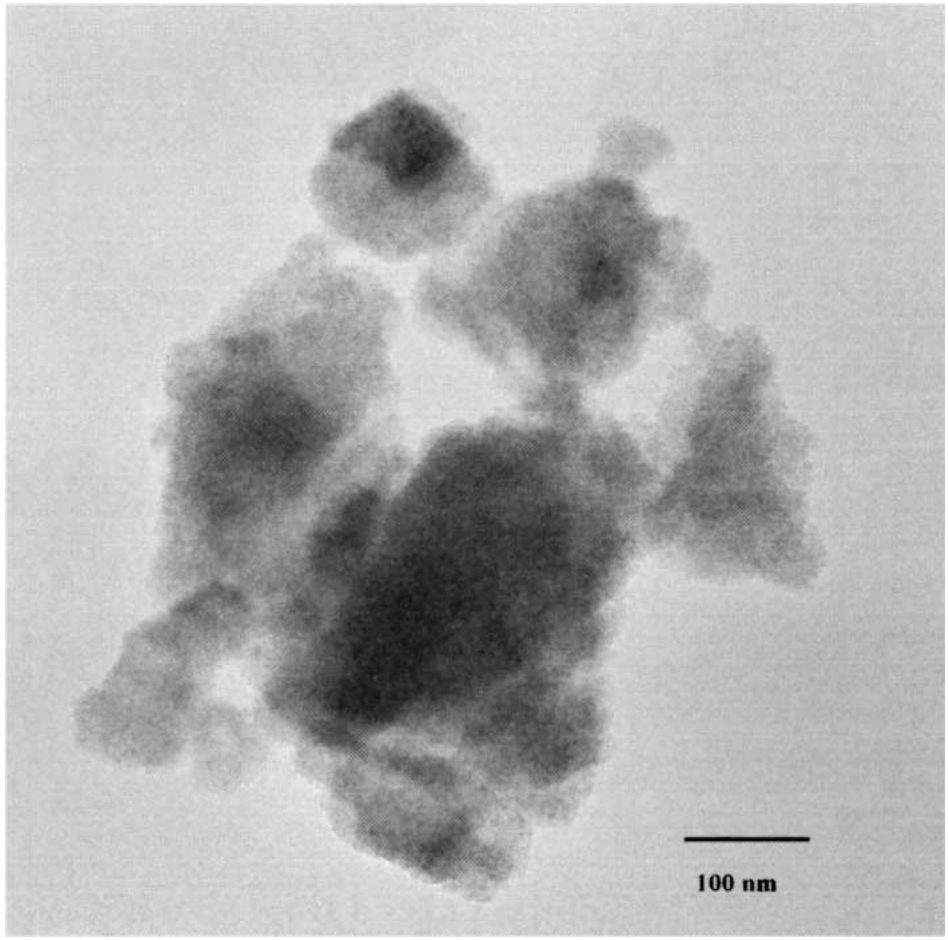

(a)

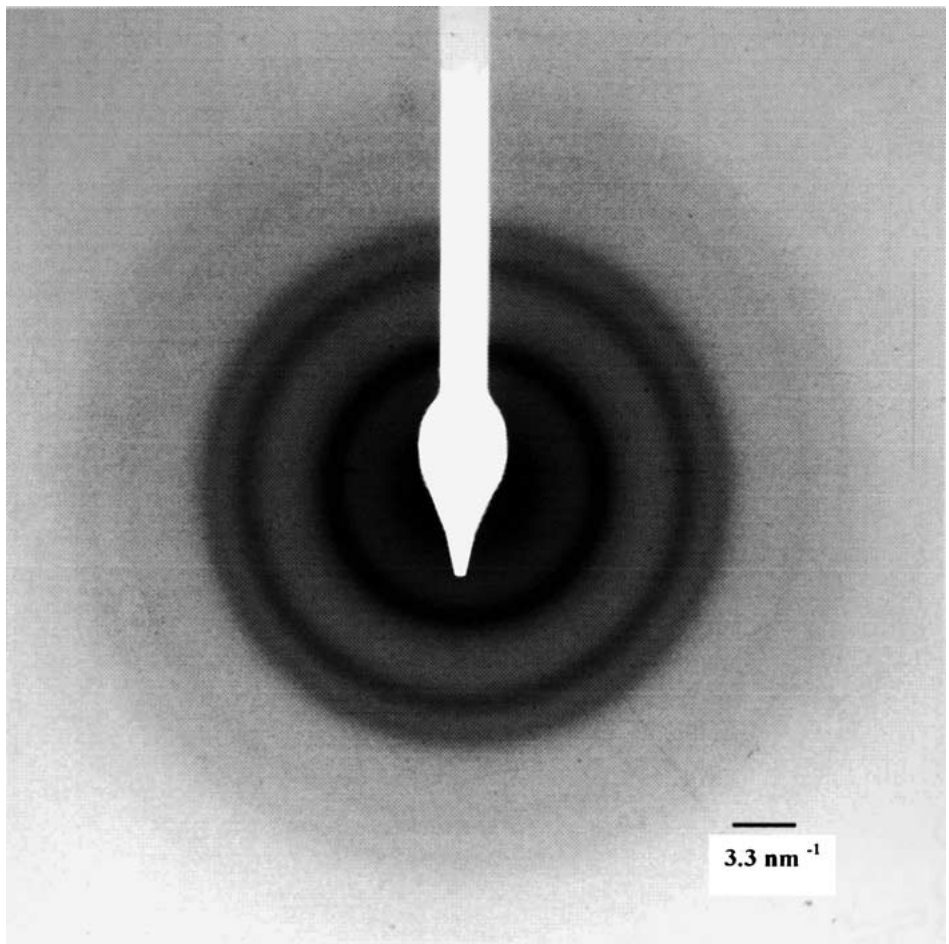

(b)

Figure 6 (a) Low resolution TEM of ZnS-1 sample.(b) Electron diffraction of ZnS-1 sample. (c) High resolution TEM of ZnS-1 sample. (*Continued.*)

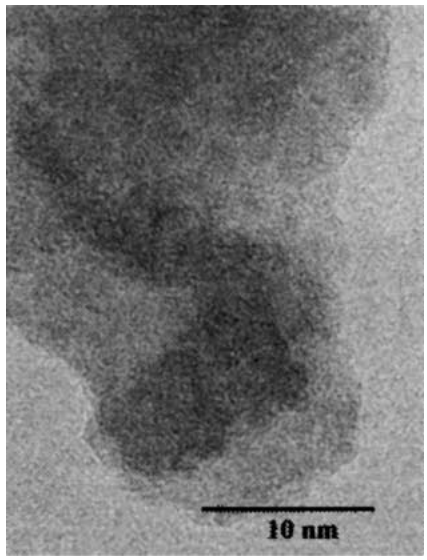

(c)

Figure 6 (*Continued*).

(CA) [36], in which many particles diffuse and stick together to form clusters which also diffuse and stick yielding self-similar aggregates with $D_f = 1.78$. A modification of CA called "reaction-limited cluster-cluster aggregation" (RLCA) uses an interparticle interaction potential in the simulation, which is intermediate in height and allows the aggregation to proceed at a much retarded rate, with many encounters before sticking. Brown and Ball [37] have achieved good agreement with the results of Schaefer *et al*. [33], ending at a fractal dimension of $D_f = 2.11$. Lin *et al*. [38] proved the universality of these two processes on three different colloidal systems and computer simulations. Beelen *et al*. [39] have reported simulated fractal dimensions of 2.1 on diffusion limited cluster-cluster aggregation with reaction constraints. Particle coalescence and rearrangement after sticking is thought to explain the more compact structure and a higher fractal dimension in some experiment [40]. This could be the origin for the higher fractal dimension of 2.7 observed for the smaller particles of sample ZnS-1.

In a simplified approach, without considering details of the correlation function between the basic scattering objects [28], the intensity scattered by mass-fractals can be expressed as $I(b) \propto I_0(b) b^{-D\mathrm{m}}$. Here $I_0(b)$ represents the structure factor of the basic scattering unit. In fact this equation describes qualitatively the observed behavior of the diffraction curve (see solid line in Fig. 4b). For this calculation the structure factor of the basic unit was defined by the scattering function of a tetrahedral fragment $Zn_{20}S_{35}$ of the cubic ZnS structure as will be discussed in the following part (see Fig. 5). However, this simplified equation does not explain the inflection point observed in the experimental curve.

One can estimate the length scale for which the aggregate is a mass fractal from the b-scale limits within which the linear slope is observed [27]:

$$1/2\pi b_{\max} < L_{\mathrm{m}} < 1/2b_{\min}$$

These limits can only be estimated since they are not well defined. From Fig. 4 we obtain the fractal length scale in the range $16\,\text{Å} < L_{\mathrm{m}} < 160\,\text{Å}$.

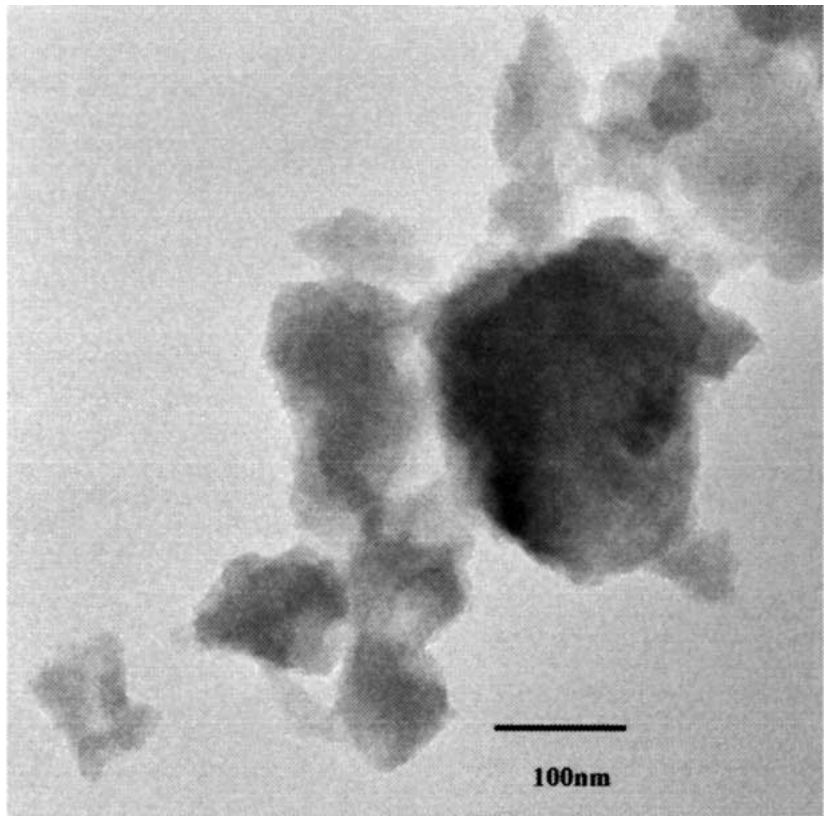

(a)

Figure 7 (a) Low resolution TEM of ZnS-3 sample. (b) Electron diffraction from ZnS-3 sample. (c) High resolution TEM of ZnS-3 sample. (*Continued*.)

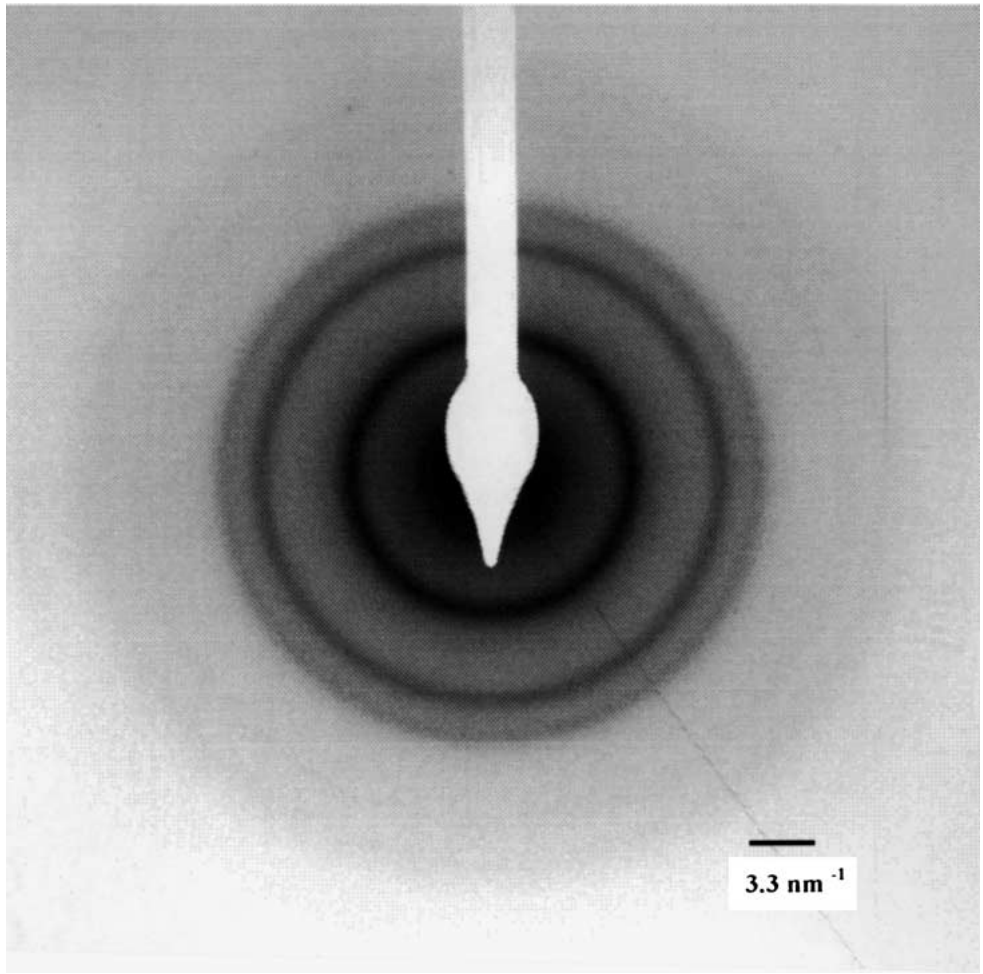

(b)

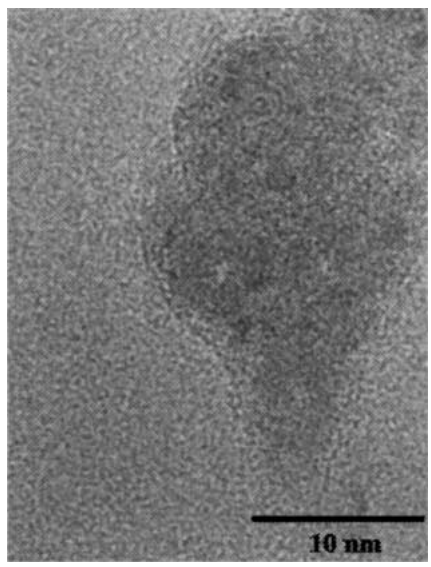

(c)

Figure 7 (*Continued*).

For a reasonable model of the nanocrystalline ZnS aggregates forming a mass fractal we can either assume (i) a strictly regular and self-similar sequence like those of the Koch pyramids [41] or more likely (ii) a network of nanocrystals, randomly linked over their edges or vertices. Ptatschek *et al*. [13] used model (i) to interpret their SAXS results on II–VI semiconductor colloids. However, from their data they were not able to prove the existence of such regular aggregates showing self-similarity. In this work we have adopted a series of tetrahedral 'closed shell' clusters Zn_mS_n, with $m_i = n_{i-1}$ and $n_i = 4, 10, 20, 35, 56\ldots, (i = 0, 1, \ldots)$ from ref. 24. Fig. 5 shows an example of four tetrahedra $Zn_{20}S_{35}$ that form a self-similar fractal object by linking them over their vertices. The next step of growth would be a super-tetrahedron build by 4 of those objects shown in Fig. 5. The building blocks Zn_mS_n have the ideal cubic sphalerite structure, where each zinc atom

is coordinated with 4 sulfur atoms. The excess sulfur atoms at the surface of the tetrahedra could be linked to the thiol-groups of the thioglycerol used as stabilizer molecules.

Strictly regular and self-similar objects would, however, lead to inter-particle interference that we do not observe in the experiment. Such an object as shown in Fig. 5a would also produce non-existing oscillations superimposed to the WAXS intensity. If, however, the basic blocks are linked via chemical bonds at their verticles to form irregular networks, then the inter-particle interference would on the average completely cancel out. The WAXS intensity remains basically unchanged, but in the SAXS range the fractal geometry produces a slope $\propto I^{-D\mathrm{m}}$ at the inner part of SAXS intensity.

In Fig. 5b-(thin line), we compare the SAXS of the fractal object of Fig. 5a with the expected SAXS of an isolated $Zn_{20}S_{35}$-tetrahedron (thick line). The latter shows the typical Porod asymptotic behavior, while the fractal object produces an oscillating SAXS signal with an average asymptotic slope close to Porod's law. If the basic tetrahedra are linked over their vertices, but randomly rotated the oscillations are reduced, and on the average would finally cancel out. This SAXS curve of the model in Fig. 5, but with random rotations is shown as dashed curve in Fig. 5. The fractal model structures discussed here are, however, too small to produce the diffraction effect of large mass fractals as those observed in the range below $b = 0.01$ Å^{-1} of Fig. 4.

From our WAXS/DFA study we know already that the basic nanoparticles are of defective crystallinity thus cannot have the morphology of regular tetrahedra, nor are they monodisperse in size. Thus we believe that the ZnS particles aggregate via reaction-limited processes to a rather dense but irregular network with $D_\mathrm{f} = 2.1$ for sample ZnS-3. For sample ZnS-1 this network is even more dense due to rearrangement processes after aggregation, leading to a larger fractal dimension $D_\mathrm{f} = 2.7$, which is already close to bulk density. (It is worth noting that as D_f approaches the value 3 the colloidal density fluctuations disappear, and accordingly the SAXS intensity tends to zero.)

The differences to ZnS-3 are seen in the smaller and less polydisperse size of ZnS-1. The larger surface to volume ratio induces a net increase of the chemical reactivity. Secondly, the smaller size and related higher mobility of the basic clusters allows for rearrangements of the pre-formed aggregates into a more compact state. These conclusions are supported by TEM-results.

Fig. 6a shows an overview image with low magnification i.e., 135 000×, of sample ZnS-1. The corresponding electron diffraction for this sample is given in Fig. 6b. From the electron diffraction it can be concluded that the structure is that of Sphalerite, i.e., cubic. The lattice parameters, thereof obtained are: $d_{111} = 0.296$ nm, $d_{220} = 0.181$ nm and $d_{113} = 0.155$ nm. In Fig. 6c the High Resolution Transmission Electron Microscope (HRTEM) image with high magnification, i.e., 495 000×, is given. It can be seen that large aggregates up to more than 100 nm diameter consist of smaller crystalline sub-domains of less than 5 nm.

Fig. 7a–c show an image of low magnification, i.e., 57 000×, electron diffraction and a HRTEM image with 495 000× magnification respectively for sample ZnS-3. From the electron diffraction the following lattice parameters are obtained: $d_{111} = 0.296$ nm, $d_{220} = 0.181$ nm and $d_{113} = 0.113$ nm as in sample ZnS-1. The structure again is Sphalerite, cubic. The sample also consists of large aggregates with small crystalline sub-domains. However, as in sample ZnS-1 it is difficult to give data on their sizes. It is estimated that the diameters are smaller than 5 nm.

4. Conclusions

Thiyoglycerol capped ZnS nanoparticles aggregate via reaction limited process to form a dense but irregular network. Smaller particles are more dense than the larger of the two nanoparticles samples due to more rearrangement of aggregates. However both the samples show the presence of particles with mass fractal dimensions being different from each other.

Acknowledgement

SKK would like to thank IUC-DAEF for the financial support. It is also a great pleasure to thank Dr. Ramnadham, BARC, Mumbai, Dr. B. A. Dasannacharya, Director, IUC-DAEF and Dr. P. S. Goyal, Centre Director, IUC-Mumbai for useful discussions.

References

1. L. E. BRUS, *J. Chem. Phys.* **80** (1984) 4403.
2. A. P. ALIVISATOS, *ibid.* **100** (1996) 13226.
3. H. WELLER, *Adv. Mat.* **5** (1993) 88.
4. S. V. GAPONENKO, "Optical Properties of Semiconductor Nanocrystals" (Cambridge Univ. Press, Cambridge, UK, 1998).
5. T. ANDO, Y. ARAKAWA, K. FURUYA, S. KOMIYAMA and H. NAKASHIMA (eds.), "Mesoscopic Physics and Electronics" (Springer, Berlin, 1998).
6. W. VOGEL, J. URBAN, M. KUNDU and S. K. KULKARNI, *Langmuir* **13** (1997) 827.
7. H. GLEITER, *Prog. Mater. Sci.* **33** (1989) 223.
8. C. B. MURRAY, C. R. KAGAN and M. G. BAWENDI, *Ann. Rev. Mat. Sci.* **30** (2000) 545.
9. *Idem.*, *Science* **270** (1995) 1335.
10. L. SPANHEL and M. A. ANDERSON, *J. Am. Chem. Soc.* **112** (1990) 2279.
11. B. A. KORGEL and D. FITZMAURICE, *Phys. Rev.* B **59** (1999) 14191.
12. C. R. KAGAN, C. B. MURRAY and M. G. BAWENDI, *ibid.* **54** (1996) 8633.
13. V. PTATSCHEK, T. SCMIDT, M. LERCH, G. MULLER, L. SPANHEL, A. EMMERLING, J. FRICKE, A. H. FOITZIK and D. LANGER, *Ber. Bunsenges. Phys. Chem.* **102** (1998) 85.
14. S. MAZUMDAR, D. SEN, P. U. M. SASTRY, R. CHITRA, A. SEQUEIRA and K. S. CHANDRASEKARAN, *Phys. Condens. Matter.* **10** (1998) 9969.
15. A. B. JARZEBSKI, J. LORENC and L. PAJAK, *Langmuir* **13** (1997) 1280.
16. V. BOCK, A. EMMERLING, R. SALIGER and J. FRICKE, *J. Porous Mat.* **4** (1997) 287.
17. I. KRAKOVSKY, H. URAKAWA, K. KANJIWARA and S. KOHJIYA, *J. Non Cryst. Sol.* **31** (1997) 231.
18. P. W. SCHMIDT and R. HIGHT, JR. *Acta Cryst.* **13** (1960) 480.
19. S. M. SZE, "Physics of Semiconductor Devices" (Wiley East. Ltd., 1981).
20. W. VOGEL, *Cryst. Res. Tech.* **33** (1998) 1141.
21. V. GNUTZMANN and W. VOGEL, *J. Phys. Chem.* **94** (1990) 499.
22. W. VOGEL, B. ROSNER and B. TESCHE, *ibid.* **97** (1993) 11611.

23. N. HARTMANN, R. IMBIEHL and W. VOGEL, *Catal. Lett.* **28** (1994) 373.
24. W. VOGEL, P. H. BORSE, N. DESHMUKH and S. K. KULKARNI, *Langmuir* **16** (2000) 2032.
25. W. VOGEL, J. BRADLEY, O. VOLLMER and I. ABRAHAM, *J. Phys. Chem.* B **102** (1998) 10853.
26. R. HOSEMANN and S. N. BAGCHI, "Direct Analysis of Diffraction by Matter" (North-Holland, Amsterdam, 1962) p. 587.
27. A. GUINIER, *Ann. Phys.* **12** (1939) 161.
28. P. W. SCHMIDT in "The Fractal Approach to Heterogeneous Chemistry," edited by D. Avnir (John Wiley, New York 1989) p. 67.
29. J. E. MARTIN and A. J. HURD, *J. Appl. Cryst.* **20** (1987) 61.
30. G. POROD, *Kolloid-Z* **124** (1951) 83; *Idem.*, *ibid.* **125** (1952) 51; *Idem.*, *ibid.* **125** (1952) 108.
31. W. RULAND, *J. Appl. Cryst.* **4** (1971) 70.
32. H. D. BALE and P. W. SCHMIDT, *Phys. Rev. Lett.* **53** (1984) 596.
33. D. W. SCHAEFER, J. E. MARTIN, P. WILTZIUS and D. S. CANNELL *ibid.* **52** (1984) 2371.
34. D. W. SCHAEFER and K. D. KEEFER, *ibid.* **56** (1984) 2199.
35. T. A. WITTEN and L. M. SANDER, *ibid.* **47** (1981) 1400; *Idem.* B **27** (1982) 5686.
36. P. MEAKIN, *Phys. Rev.* A **27** (1983) 1495.
37. W. D. BROWN and R. C. BALL, *J. Phys.* A **18** (1985) L517.
38. M. Y. LIN, H. M. LINDSAY, D. A. WEITZ, R. C. BALL, R. KLEIN and P. MEAKIN, *Nature* **339** (1990) 360.
39. T. P. M. BEELEN, W. H. DOKTER, H. F. VAN GARDEREN and R. A. VAN SANTEN, *Adv. Colloid Interface Sci.* **50** (1994) 23.
40. P. MEAKIN and R. JULLIEN, *J. Phys. (Paris)* **46** (1985) 1543.
41. B. B. MANDELBROT, "The Fractal Geometry of Nature" (W. H. Freeman, New York, 1983).

Received 10 January
and accepted 18 July 2002